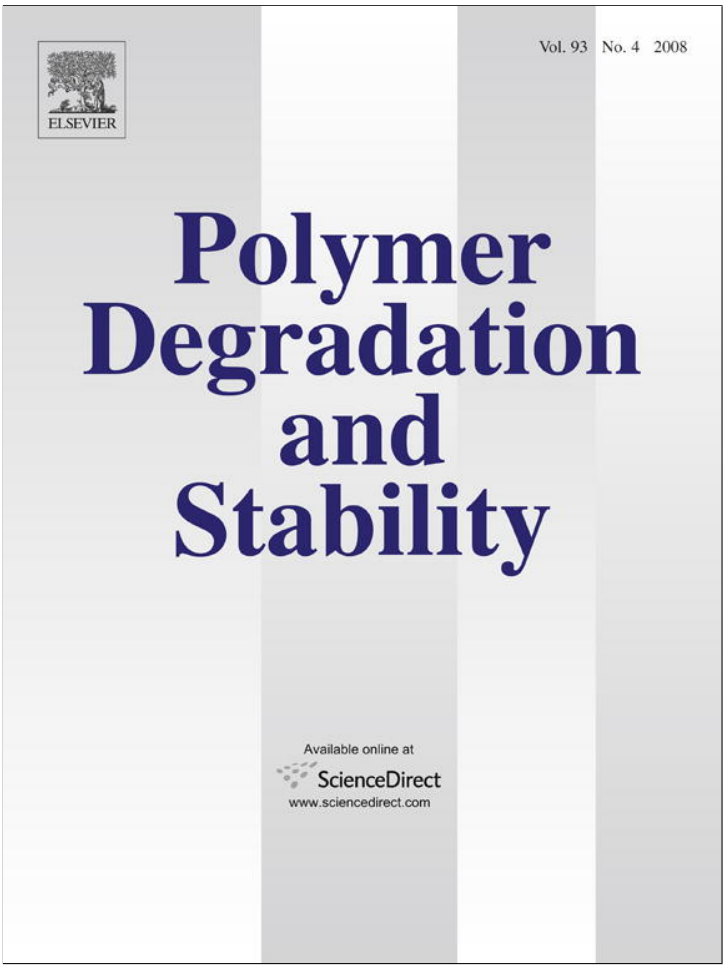

Available online at www.sciencedirect.com
ScienceDirect
Polymer Degradation and Stability 93 (2008) 827–837
Polymer Degradation and Stability
www.elsevier.com/locate/polydegstab

Nanoscale degradation of polypyrrole films under oxidative stress: An atomic force microscopy study and review

Jorge G. Ibanez [a,*], Alejandro Alatorre-Ordaz [b], Silvia Gutierrez-Granados [b], Nikola Batina [c]

[a] *Centro Mexicano de Quimica en Microescala, Departamento de Ing. y Ciencias Quimicas, Universidad Iberoamericana, Prol. Paseo de la Reforma 880, 01210 Mexico, D.F., Mexico*
[b] *Instituto de Investigaciones Científicas, Universidad de Guanajuato, Cerro de la Venada s/n, Pueblito de Rocha, Guanajuato, Gto, Mexico*
[c] *Universidad Autónoma Metropolitana-Iztapalapa, Departamento de Química, Av. Michoacan y la Purisima, Col. Vincentina, Apdo. Postal 55-534, 09340 Mexico, D.F., Mexico*

Received 21 November 2007; accepted 10 January 2008
Available online 17 January 2008

Abstract

Atomic force microscopy (AFM) is employed to monitor the surface morphology of polypyrrole (PPy) films grown on vitreous carbon substrates during the catalytic reduction of Cr(VI) to Cr(III). The morphology of freshly-prepared films depends on substrate characteristics. Upon reaction, uniform nodules of aggregated PPy clusters appear. No significant differences in surface morphology are found between its oxidized and reduced forms. Loss of catalytic activity after 8–9 oxidation/reduction cycles of exposure to the chromate solution (oxidation) and electrochemical recharging of the film at negative potentials (reduction) correlates well with the observed polymer film dissolution/detachment from the carbon substrate. Formation of well-defined circular features (PPy rings) at different stages leads to a model for the film degradation process that includes formation of Cl_2 gas inside the polymer matrix. In the final stages, the bulk of the film typically fractures and detaches from the electrode. A catalytically inactive, ultrathin PPy layer remains on the substrate even after prolonged exposure to the target solution. A review of techniques for the study of PPy aging/degradation is given.

Keywords: Polypyrrole degradation; Atomic force microscopy; Polymer degradation; Oxidative degradation

1. Introduction

Selected properties of conducting polymers make them suitable for a variety of applications. In the case of polypyrrole (PPy), useful features include its capacity to form adhesive coatings at different substrates, the possibility of growing it in aqueous media, easiness for chemical substitution to modify its properties, high porosity that enables ion exchange with the surrounding medium, high electronic conductivity, high chemical stability, thickness controllability, ease of electrochemical polymerization, and good reversibility between its conducting and insulating states. As a result, PPy has found applications in fields like rechargeable batteries, chemical and biochemical sensors, super capacitors, electromagnetic shielding, microelectronic and electrochromic devices, corrosion protection, antistatic packaging materials, and separation barriers. Such a plethora of applications have made their production technology and the study of their properties relatively well known.

Cr(VI) ions are highly mobile and toxic [1,2], and processes have been sought to reduce them to the much less dangerous and easily precipitable Cr(III) moieties [3–11]. The direct reduction of Cr(VI) on bare electrode surfaces may suffer from limited electron transfer kinetics and selectivity problems [12,13] (although fitting conditions can be found in selected reports, see for example Refs. [14–16]). This has prompted the search for catalyzed alternatives, one of which involves the use of PPy modified carbon electrodes [12,13]. Here, the Cr(VI) reduction is based on a spontaneous electron transfer to Cr(III) ions from a pre-reduced conducting polymer

* Corresponding author. Tel.: +52 55 59504074; fax: +52 55 59504279.
E-mail address: jorge.ibanez@uia.mx (J.G. Ibanez).

0141-3910/$ - see front matter © 2008 Elsevier Ltd. All rights reserved.
doi:10.1016/j.polymdegradstab.2008.01.009

film. Schematically, the process can be illustrated by the following reactions:

$$Cr_2O_7^{2-} + 6PPy(0) + 14H^+ \rightarrow 2Cr(III) + 6PPy^+ + 7H_2O \quad (1)$$

and

$$PPy^+ + e^- \rightarrow PPy(0) \quad (2)$$

where PPy(0) and PPy^+ correspond to the reduced and oxidized states of the PPy film, respectively. Thermodynamic, kinetic, mechanistic and catalytic aspects of these two processes have been studied in detail [12,13,17–19]. During this catalytic reaction negative Cr(VI) ions physically penetrate into the PPy film, where they are reduced and released into the solution as positive Cr(III) due to an ion exchange mechanism [12]. This process is complemented by a positive charging of the neutral PPy film. To compensate for the resulting positive charges and to sustain ion exchange, solution anions are adsorbed and uptaken into the PPy film. PPy film deactivation and stability over repeated cycles in Cr(VI) containing solutions [17,19] may be related to physical degradation of the PPy film and/or to changes in its electronic-physicochemical properties like ion exchange and kinetics [18]. This problem is rather complex since many processes are involved in the overall reaction scheme, both from the side of the PPy surface and of the solution. The purpose of the present study is to contribute to the elucidation of this problem.

Common ambient substances (e.g., acids/bases, redox species, water, and organic vapors) can react with PPy or be incorporated into it (e.g., non-reactive ions and surfactants). These processes may change its polymeric structure/composition and degrade it [20]. Various artificial conditions (e.g., an externally applied potential) may degrade PPy as well [21–25].

The simplest and most common technique for monitoring PPy degradation or aging is electrical conductivity, as it may examine changes in bonding and structure, degree of oxidation, degradation kinetics and mechanism, and concentration of key charged species [25–34]. Conductivity usually accompanies other (more powerful) techniques. For instance, the oxidative degradation of PPy involves a decrease in conductivity due to the formation of C–Cl bonds in the pyrrole ring structure, as demonstrated by ^{13}C NMR [35].

Due to the importance of the study of PPy degradation, a brief review of other techniques employed for this purpose is given below.

- Structural modifications of doped PPy films during undoping–redoping processes are monitored using spectroscopic techniques and elemental analysis. Key changes at the pyrrole nitrogen can be quantified. Degradation results from the loss of effective conjugation in the polymer due to reactions of the pyrrole rings with oxygen or oxygen containing groups. Changes are attributed to the way in which the anions are incorporated into the polymer matrix and to the mobility of the anions during the undoping–redoping process [36]. The degradation of PPy by anodic oxidation in aqueous solution is followed by UV, IR, NMR, and mass spectra of the degradation products, which are mainly found to be a mixture of maleimide and succinimide [24]. Electronic spectroscopy reveals interactions between attacking agents and the bipolaron and polaron defects [37]. Fourier transform infrared spectroscopy (FTIR) studies the stability of PPy towards ozone attack [37]. FTIR and reflectance FTIR can help in the elucidation of degradation mechanisms by analyzing changes in the intensity and wavelength of absorption bands due to the formation of hydroxyl, nitrile and carbonyl species [25,27,30]. In situ FTIR provides information on the molecular changes resulting from generation of charge carriers in the PPy conjugated heterocyclic system during its oxidative degradation in aqueous solution. Examples include the generation of radical cations and dications produced by the application of an external potential; nucleophilic attack of OH^- ions (originating from the dissociation of the solvent); formation of carbonyl and hydroxyl groups; CO_2 formation; and interactions between ions and charge defects in the backbone [22].
- In situ time-resolved Raman (TRR) studies redox process and the degeneration of PPy as a function of pH. Peak shifts (coupled to cyclic voltammetric data) help to understand mechanistic details by detecting unstable intermediates related to protonated, oxidized PPy [38].
- Positron annihilation spectroscopy (PAS) probes aging-induced changes in doped PPy by analyzing positron trapping in the vicinity of negative dopants whose concentration changes upon aging [28].
- The application of X-ray techniques for the study of PPy degradation includes X-ray photoelectron spectroscopy (XPS) that analyzes the concentration of C:N bonds; this reflects the number of defects in the chemical structure of the polymeric backbone [26,34]. Surface change features of PPy can also be characterized using synchrotron-based X-ray photoemission electron microscopy (X-PEEM) [39]. Near edge X-ray absorption fine structure (NEXAFS) analyzes electronic states and changes upon irradiation (including overgrowth of PPy and formation of PPy granules) [39].
- The oxidative degradation of doped PPy films can be investigated by thermal analysis including differential scanning calorimetry (DSC), thermogravimetric analysis (TGA), and differential thermal analysis [34,37].
- The stability of PPy towards oxidation can be explored by weight increase measurements [37].
- The electroactivity of PPy films is degraded by applying anodic potentials that produce its overoxidation. Voltammetry and chronoamperometry reveal decreasing diffusion coefficients due to an increasing degree of crosslinking between neighboring polymeric chains. This reduces conjugation lengths and increases the rigidity of the conformational electro-chemo-stimulated movements on the chains due to the formation of rigid and oxidized islands entrapped by crosslinking points that prevent any ionic

interchanges [21]. The rate of the electrochemical degradation of PPy increases with potential [40]. In fact, the application of a potential takes the PPy from its reduced, insulating state, through its oxidative degradation [22]. Kinetic measurements of the degradation of PPy films in aqueous solution are obtained by applying proper potentials and monitoring the absorbance of the electrolysis products as a function of time. Films degrade faster at higher degradation potentials, at higher acid concentrations, and when they are thinner [23]. Evolution of physical and electrochemical properties of PPy during anodic oxidation is also monitored by cyclic voltammetry and in situ quartz microbalance experiments [24,25,38]. The charge storage capacity changes are significant [25].

- Changes in tensile properties and microwave shielding are used for inspecting the aging of doped and undoped PPy films. Microwave shielding shows that stable films retain better their high microwave reflectivity [27].
- Inverse gas chromatography (IGC) examines PPy degradation by its changes in surface energy [26].
- Evolved-gas analysis (EGA) monitors thermal aging of Cl-doped PPy powder through the evolution of CO, CO_2, H_2O and NH_4Cl that results in ring-opening reactions and the formation of oxidized species. The latter shortens the conjugation length leading to a rapid loss of conductivity (due in part to water production). These PPy degradation mechanisms are rather complex [30].
- Microscopy is an obvious choice to study surface phenomena during PPy degradation. For instance, scanning electron microscopy (SEM) follows changes in morphology during aging processes of PPy [31] and its oxidative degradation [34]. Atomic force microscopy (AFM) verifies the topography of pattern growth [39] and is a useful tool for analyzing nano- and micro-sized features and events on different kinds of surfaces. By using AFM the need of exposing the sample to a vacuum is circumvented, which can be important for the visualization of soft surfaces.

In view of the above considerations, we set out to study PPy stability and durability during the chromate process described earlier by monitoring its surface morphology with AFM with the objective of identifying key parameters and events. Since PPy films grown by electrochemical techniques in the presence of bromide or iodide ions possess a greater capacity for Cr(VI) reduction than those grown in the presence of chloride or fluoride ions [41], the study of PPy reacting with Cr(VI) in the presence of chloride ions may shed light on its degradation process, as shown below.

2. Experimental section

An AFM, Nanoscope III − (Digital Instruments) was used in the contact mode, under normal laboratory air atmosphere and using standard geometry silicon nitride probes (Digital Instruments). The scan rate was 1−2 Hz. The PPy film was brought in contact with the chromium solution in cycles up to its visible degradation. Three replicate samples were prepared and tested for each experiment. No destruction of the sample surface was noticed during imaging. All images are presented in the height mode, where the higher parts appear brighter.

PPy films were potentiostatically grown on vitreous carbon disks (GICR-10, Electrosynthesis Co., 10 mm diameter) at a constant potential of 0.9 V (vs. Ag/AgCl) from aqueous solutions containing 0.1 M pyrrole (Aldrich) and 0.1 M KCl (Aldrich). The film thickness and the amount of polypyrrole on the support electrode were controlled by the charge consumed in the electrosynthesis. Layers of different thickness were prepared by varying the time of the electrosynthesis process (i.e., electrodeposition time) from 5 s to 5 min. (For thicker films, longer preparation times were required.) After preparation, each electrode was transferred to a pyrrole-free solution and a voltammogram was plotted to verify the presence of the polymer on the electrode. Before use the vitreous carbon disks were polished with 0.3 μm alumina powder, ultrasonicated during 10 min in a 1% H_2SO_4 solution, and rinsed with pure water. Electric contact to the disks was made to the opposite end of the working surface with a Pt wire glued with a conductive paint (ACME Chemicals & Insulation Co.). During polymer film formation, potentials were controlled with a Bioanalytical Systems CV-27 potentiostat (BAS) coupled to an AMEL 2051 potentiostat. The auxiliary electrode was a graphite rod with a surface area much larger than that of the working electrode. Prior to PPy synthesis, the solution was carefully deaerated with high purity nitrogen gas. All potentials reported here are referred to the Ag/AgCl (in 3 M KCl) reference electrode. All solutions were prepared from analytical grade reagents, using deionized or doubly-distilled water.

After preparation, each film was characterized by AFM and conditioned (i.e., recharged) for the catalytic reaction with chromate solution. This involved reduction at −0.9 V for 15 min in a pyrrole-free 0.1 M KCl solution. Once thoroughly washed with DI water, the reduced film was brought in contact with a 100 ppm Cr(VI) (as K_2CrO_4) in 0.1 M H_2SO_4 solution in an open beaker without the application of an external potential. After 90 min of contact with the chromate solution, the PPy film surface was AFM imaged. Identical cycles (always using fresh chromate solution) were repeated until obvious polymer degradation was observed. An optical microscope (Carl Zeiss, model 464026, Germany) coupled to a photographic camera was employed for visualization of macroscopic changes in surface morphology.

Chloride ion analysis was performed using an Ion Chromatograph (Dionex, model 2020i) with an HPIC-AS4 column.

3. Results and discussion

3.1. Surface morphology of potentiostatically grown PPy films prior to contact with Cr(VI)

Although PPy grown on porous substrates offers a much greater reaction surface [42], it is very difficult to image by AFM. Thus, we grew PPy on a flat vitreous carbon disk.

As a preliminary step the clean vitreous carbon surfaces were imaged. Fig. 1 shows AFM images of mirror-polished vitreous carbon substrates; on the larger scale image (15 μm × 15 μm) characteristic footprints of a polishing procedure in the form of long scratches (0.03–0.05 μm wide and ca. 15 nm deep, see Fig. 1a) can be noticed. Fig. 1b shows higher resolution images (1 μm × 1 μm), which reveal that the flat substrate consists of small nodule-like features (diameter: 50–70 nm) that appear to be ordered along the polishing lines. Such morphology is in good agreement with previous findings using STM [43,44]. Fig. 2 shows AFM images of PPy films grown during 5 s (Fig. 2a) and 20 s (Fig. 2b). They possess different morphological characteristics. Contrary to the 20 s-film, the 5 s-film appears very uniform and consists of a large number of rather small individual grains (i.e., distinct nodular protrusions). The average diameter of the individual grains is ca. 60–70 nm. PPy film-coated samples (with estimated thickness of 0.2–0.4 μm) appeared greenish with typical polishing stripes present over the film surface. These findings are indicative of a significant influence of the carbon substrate morphology on the early stages of the PPy film growth (i.e., an ultrathin film). We also prepared PPy films using graphite substrates instead of vitreous carbon and found significantly different surface morphologies. In both cases the ultrathin PPy film closely tracked the substrate's surface morphology.

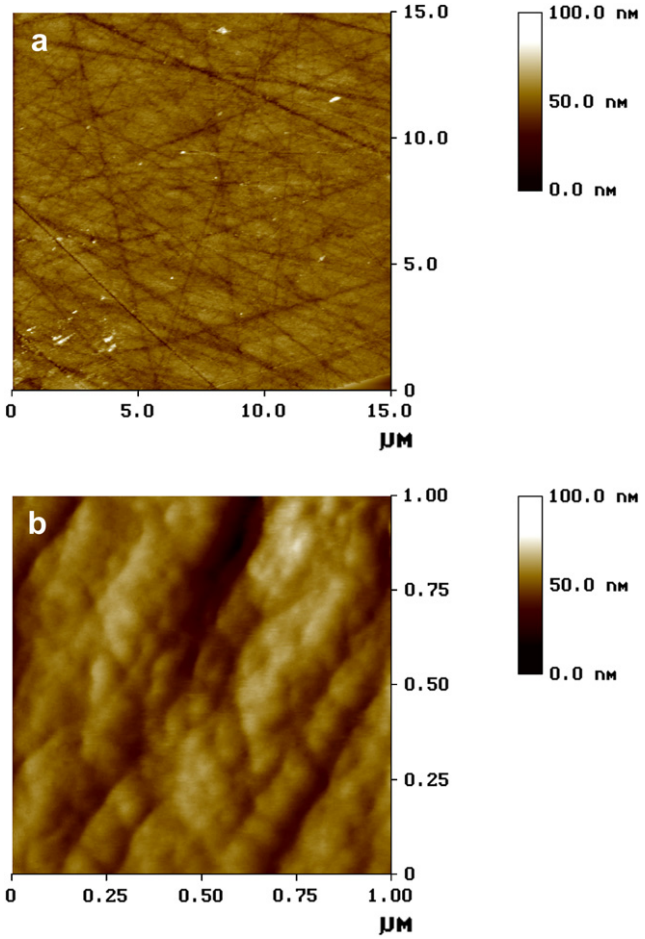

Fig. 1. (a) AFM image (15 μm × 15 μm) of a freshly-polished vitreous carbon electrode surface, showing typical polishing scratches. (b) High resolution AFM image (1 μm × 1 μm) revealing a nodule-like substrate superstructure. *Z*-range in both images: 0–100 nm.

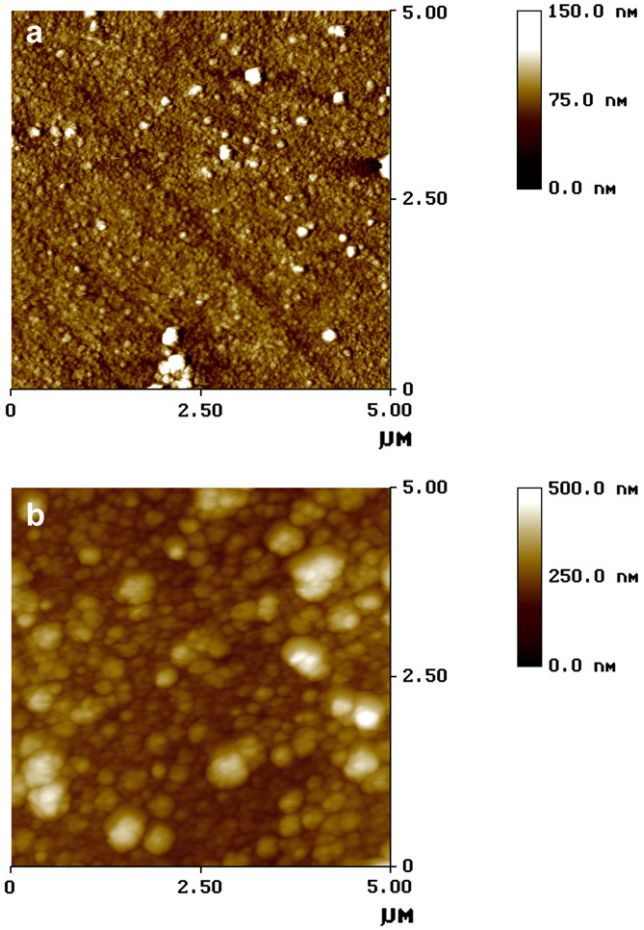

Fig. 2. Typical surface morphology of the PPy film grown on a vitreous carbon substrate during 5 s (a), and 20 s (b). AFM images (5 μm × 5 μm) were taken directly after PPy synthesis. The *Z*-range varies from 0 to 150 nm (a), and from 0 to 500 nm (b).

Contrary to the 5 s-film, the 20 s-films are largely formed by bulky polymer grains (diameter up to 0.5 μm), clearly signaling a polymer agglomeration process (see Fig. 2b). In addition to these large aggregates, the rest of the film surface shows grains with an average size of ca. 0.28 μm. This image does not indicate an influence of the substrate morphology. In fact, surface morphology observed on the image is very similar to published scanning electron micrographs of electrochemically-grown PPy films [45], typical of thick polymer films. With even longer electrosynthesis times, agglomeration of PPy grains becomes a characteristic trend. For example, in a 300 s-film, huge 3-D features completely covered the electrode surface. The sample appeared black (with a film thickness of ca. 1.5–1.7 μm). Due to the height of the surface features (i.e., more than 4 μm), such samples became out of range for AFM analysis. In order to check the stability of such PPy films, we probed the same samples during a period of several weeks. No changes were noticed in the AFM images during this period. Samples were stored between examination cycles in a beaker under air laboratory atmosphere and at room temperature.

PPy film morphology was also monitored as a function of its redox state in the conductive (oxidized) and non-conductive (neutral), reduced state [46]. Prior to contact with the chromate solution, the polymer naturally switched from the neutral to the positive state. This switching is accompanied by a color change from a dark-green (oxidized polymer) to light yellow (neutral polymer). Nonetheless, AFM revealed that no significant changes in the surface morphology of the PPy film between the oxidized and reduced forms occurred.

We also monitored the stability of reduced PPy films in the electrolyte solution subject to negative potentials. Under such conditions, the reduced (neutral) PPy film was brought in contact with a Cr(VI) solution. Different samples (i.e., 5 s-, 20 s- and 5 min-films) were subjected to a potential of −0.9 V during longer periods of time (up to 30 min). Selected samples were also repeatedly subject to this potential −0.9 V in time increments of 15 min, up to 17 cycles. After each exposure, each sample was taken out of the KCl solution, rinsed with pure water, dried in air, and then inspected by AFM. For the next cycle, each sample was re-immersed in the KCl solution at the control potential of −0.9 V. AFM images showed no noticeable changes in the surface morphology during such experiments, which is an indication of the high stability of the PPy film in the reduced, insulated form.

3.2. Degradation of PPy films: AFM visualization

Polymer films of different thickness showed different endurance towards the degradation process. Samples with larger amounts of polymeric deposit (e.g., the 5 min-film) stand out ca. 9 cycles before the polymer cracks and peels off from the vitreous carbon substrate. The peeling is visible to the naked eye. Analysis of such samples with AFM was not possible due to the rough surface features, which were outside the detection limit of the AFM technique (*Z*-range movement). However, some images obtained at the flattest parts of the electrode surface show that the polymer film undergoes a slight decrease in particle size during the subsequent cycles (i.e., chromate exposure and regeneration). After the 6th to 7th cycle, small gas bubbles trapped in the region between the polymer and the substrate surface were evidenced by the polymer's bubble-like expansion. Since cracking and disengaging of the polymer film from the electrode surface primarily occurs at the film/substrate interface, it is logical to suppose that this was due to evolution of a gaseous species.

A rather different behavior was observed with ultrathin PPy films grown during only 5 or 20 s. Instead of an abrupt detachment of the polymer film from the substrate, a step-by-step film dissolution was observed. Due to the higher film smoothness, surface morphology changes were followed by AFM images of the 5 s- and 20 s-films more easily. Changes were observed at very early stages of the polymer degradation (i.e., in the 3rd or 4th chromium contact cycle) in the case of the 5 s- and 20 s-films, respectively. The 5 s-film appears to be more vulnerable to the degradation process than the 20 s-film (see Fig. 3). This image shows the top surface layer of the polymer film organized in the form of small rings

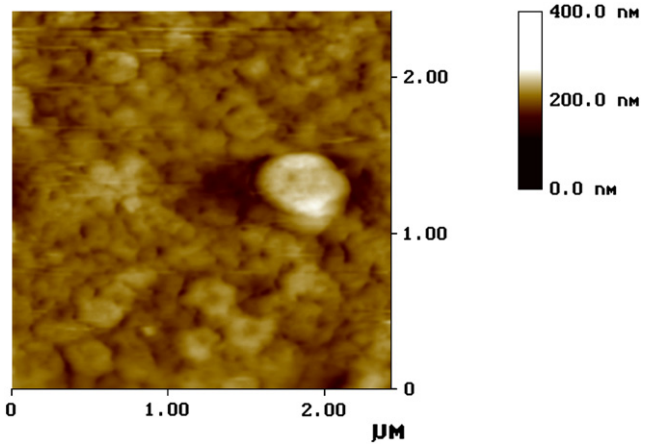

Fig. 3. Formation of ring structures on the 20 s-PPy film surface during the early stages of chromate exposure (e.g., 4th cycle). Image size: 2.4 μm × 2.4 μm. *Z*-scale: 0–400 nm.

(around 75 nm in diameter). Each ring has three or four internal protrusions that can be recognized, which is an indication that the rings were formed due to the aggregation of individual polymer grains. Imaging with higher force usually resulted in damage of the ring surface, which points at the relatively soft nature of the film.

The AFM image in Fig. 4a reveals the circular structure (phase) of a PPy film. This image was taken after the 4th cycle of chromate exposure, but the same kind of structures has been observed between the 4th and 9th cycles. Isolated circular features typically appeared randomly at the film surface. The number of circular (donut-like) features increased with each additional cycle of chromate exposure. After the 9th cycle, the polymer film was found completely covered by circular features. Detailed analysis showed that the inner and outer parts of the polymer circles possess identical surface morphology (Fig. 4b). This indicates that the bottom of the inner parts consists of polymer film, rather than the CV substrate. Since the inner part was always significantly lower than the rest of the surface (ca. 20–190 nm), these features can be considered as pinholes. In order to understand the origin and cause of these transformations we have traced the development of circular features on the polymer surface after each cycle of exposure to the chromate solution. Changes in the size, height and depth of the circular features were estimated by using AFM cross-section analysis. Fig. 5a shows an AFM image with the corresponding cross-section of three characteristic circular features (A, B, C) (Fig. 5b), which are different in overall size and area of the inner part. The diameter of the inner-circle portion as well as the thickness and height of the wall (ring) of each cycle were estimated for a large number of samples at different places. The results show the following correlations. Circular features with smaller diameters, up to 1 μm (presumably at the early stages of development) usually do not show the inner opening. On the contrary, the bigger (older) features possess the inner open part (donut-shape) whose bottom is lower than the rest of the film surface. "Donuts" with wider inner space diameter also seem to be deeper. However, no

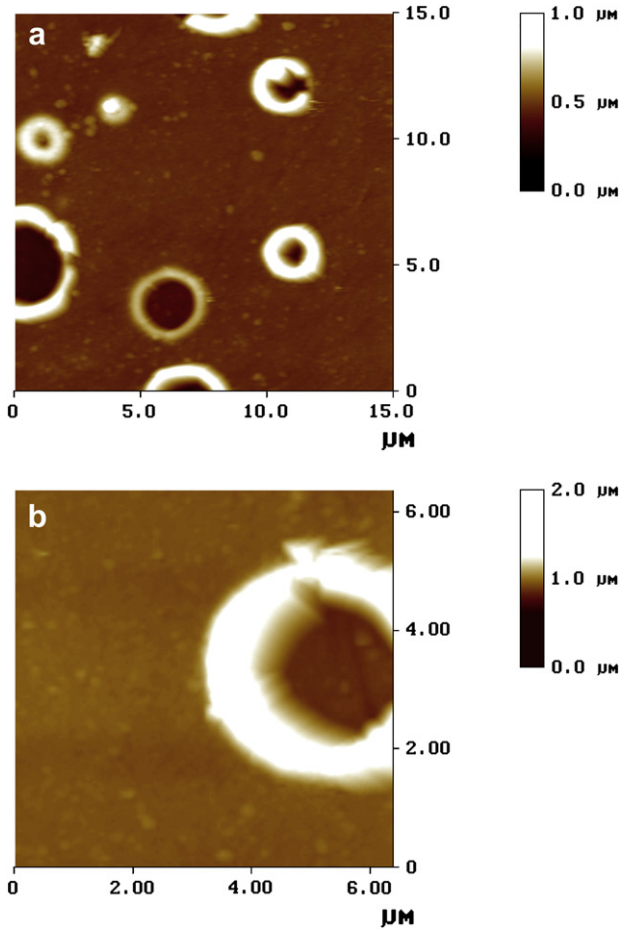

Fig. 4. (a) AFM images revealing the existence of circular features on the PPy film with the same surface morphology characteristics found inside and outside of the polymer ring. (b) Images recorded on a 5 s-film after the 4th cycle of chromate exposure. Image size: (a) 15 μm × 15 μm, and (b) 6.4 μm × 6.4 μm. *Z*-scale: (a) 0–1 μm, and (b) 0–2 μm.

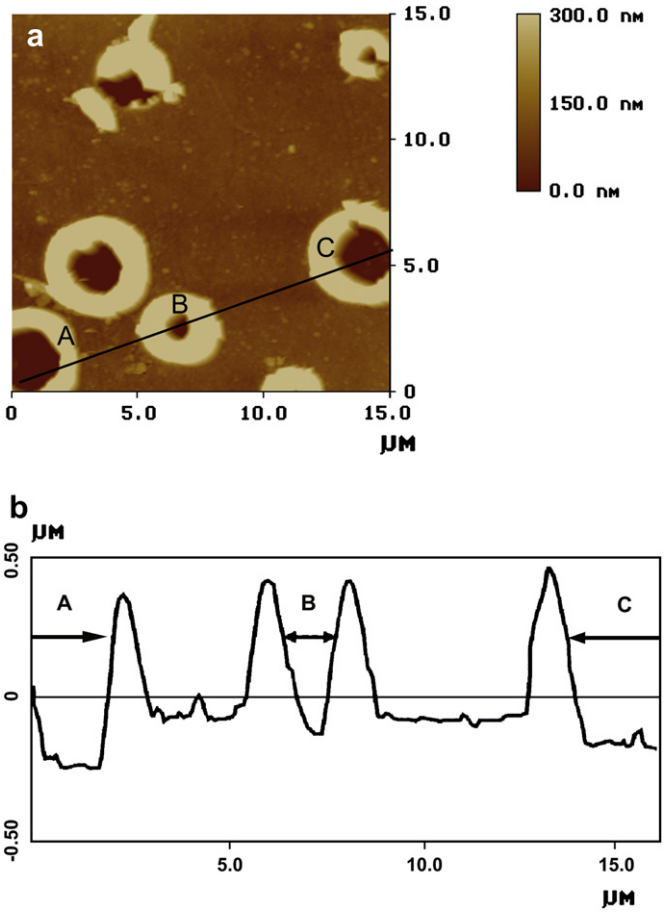

Fig. 5. 15 μm × 15 μm AFM image (a), with the corresponding cross-section over three distinguishable circular features (A, B, C) on the polymer surface (b). *Z*-scale: 0–300 nm.

features in any phase of the measurements exceeded a depth of 190 nm, which is probably related to the total thickness of the PPy film. Note that the estimation of the pinhole depths by the AFM technique may be significantly influenced by the shape of the AFM probe. The wider features with bigger diameter (presumably formed earlier) also appear to be higher (up to 700 nm). Both the outside and inside diameter of the circular features significantly increase (by a factor of 2–3) with each exposure to the chromate solution. On the 5 s-film, circular features with outside diameters between 4 and 5 μm (maximum value) were observed after the 5th chromate cycle. In the later stages (after the 7th or 8th cycles) donuts with maximum outside diameters of 10–15 μm were found. At this point, the observations of the polymer circular structures become also accessible by an optical microscope. This gives the possibility to observe a larger surface area and also clearly shows that – at any stage of development – the polymer surface possesses circular features with a variety of diameters. Obviously, this indicates the different age of the circular features, which start to grow at different times. Overlapping of growths occurring inside other previously formed circles were not observed. After 9 or more chromate cycles, the PPy film surface becomes somewhat smoother, with no indication of circular features.

Slightly thicker, 20 s-films showed a very similar pathway of changes in surface morphology as those described above for the 5 s-films. In particular, this is valid for the first 5–6 chromate cycles. The average circular features seem to be of a much larger diameter (7–10 μm), deeper (260–300 nm) and higher (ca. 600 nm) than those observed on the 5 s-film, after identical 5 cycles of chromate treatment. Significantly different developments are visible after the 6th chromate cycle, as signaled by the appearance of a new kind of semicircular features and deep cracks in the polymer film. Visualization by optical microscope indicated a partial flattening (i.e., disappearance of circular structures) and partial detachment of the polymer film from the carbon substrate (7th chromate cycle, see Fig. 6). The polymer detachment from the electrode surface becomes even more obvious after the 8th cycle. After 10 chromate cycles, the electrode surface looks flat. Even then, AFM images revealed that the carbon surface is still covered by an ultrathin layer of PPy. Small clusters of PPy could be easy recognized along the polishing scratches on the electrode surface (Fig. 7). Note that the surface morphology of this 20 s-film (even after 10 chromate cycles) does not correspond to that of the clean vitreous carbon substrate surface (Fig. 1a–c).

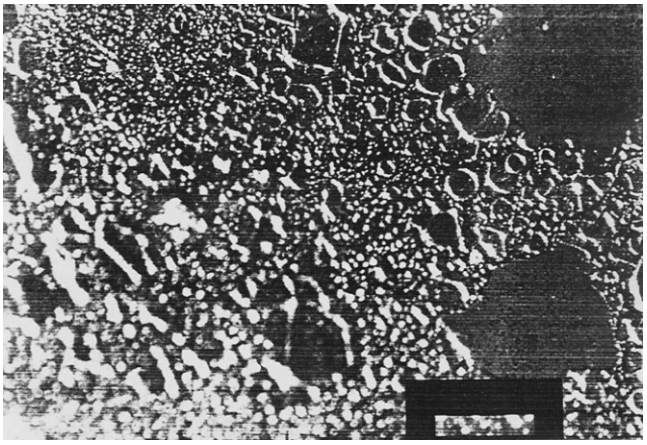

Fig. 6. Micrograph taken with an optical microscope, after the 7th cycle of chromate exposure, showing the circular structure of the PPy layer as well as two islands with almost completely removed polymer film (dark features in the lower part of the image). (The black mark corresponds to 500 μm.)

In spite of the fact that after 8 to 9 chromate cycles the PPy film had already lost its catalytic properties, we continued the chromate exposure up to 13 cycles. Even after that, PPy was not completely removed from the electrode surface, which clearly indicates that complete detachment of the PPy film from the electrode surface does not occur. This remaining film did not show catalytic activity. In other words, the catalytic activity of the PPy film towards the Cr(VI) to Cr(III) reaction is associated with the bulk properties of the PPy film (e.g., ion exchange capacity). As these results show, dissolution of the PPy film is taking place and the loss of polymer thickness is directly related to the loss of catalytic activity.

3.3. Mechanism of the PPy film degradation

As discussed earlier, uniform PPy films with a reasonably well-defined surface morphology were successfully prepared potentiostatically at the CV substrates. Their morphological characteristics have been shown to be a function of the nature

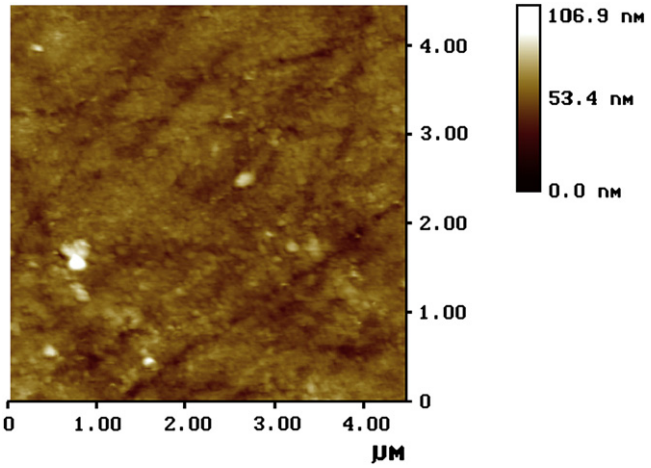

Fig. 7. Thin polymer layer consisting of small PPy clusters still remaining on the vitreous carbon substrate even after 13 chromate cycles (with no signs of circular structures). Image size: 4.5 μm × 15 μm. Z-scale: 0–107 nm.

of the substrate (in the early stages) and of film thickness (in the later stages of polymer growth). Degradation of these PPy films also depends on their thickness. For the Cr(VI) to Cr(III) catalytic conversion, thinner films (grown for 5 s and 20 s) are more appropriate since they show longer durability and no sign of massive detachment from the substrate surface, contrary to the 5 min-films. Degradation of PPy films is primarily caused by exposure to the chromate solution. Independent stability tests of the reduced and oxidized PPy forms (in the absence of chromate ions) showed no signs of polymer degradation. Analysis of surface morphology changes for the 5 s- and 20 s-films after chromate/discharging cycles revealed that polymer deterioration can be characterized as a multistep process. A schematic representation of the global process, with special emphasis on the possible explanation for the circular structure development, is shown in Fig. 8.

In particular, two steps seem to be crucial for understanding the degradation mechanism of PPy films. First, the softening and formation of "bulbs" at the polymer film surface observed in the early stages (Fig. 8b) after 4 or 5 chromate cycles. These seem to be caused by the development and expansion of gaseous species in the bulk of the polymer film (in the vicinity of the electrode surface). We suspected that the origin of this gas could be the Cl^- anion, present in our electrolyte solutions during PPy film formation and in the regeneration solution used for the polymer recharging process after each cycle of chromate exposure. Some Cl^- traces probably remain trapped in the bulk of the polymer film layers due to slow or insufficient outward ion transport. In the Cr(VI) containing solution they may be converted to the gas phase, expand and cause the polymer "bubbling" since the standard potentials of the Cr(VI) to Cr(III) and the Cl^- to Cl_2 conversion are very close to each other (1.33 and 1.35 V vs. NHE, respectively) [47]. Due to a catalytic effect on the PPy modified CV electrode, this Cr(VI)/Cr(III) conversion occurs at much lower potentials. The open circuit potential, OCP (i.e., under no potential control) of a PPy modified CV electrode immersed in 0.1 M H_2SO_4 containing 100 ppm Cr(VI) was measured to be ca. 0.85 V vs. Ag/AgCl. Indeed, during the 2 h period (which was a typical time of exposure to the chromate solution), OCP increases slightly as a result of polymer oxidation. Although the OCP is probably established as a result of the PPy film (oxidation) and chromate ions (reduction) redox reactions, under such conditions the Cl_2 evolution may be expected as well. This can happen only if the PPy film were able to catalyze the Cl^- to Cl_2 reaction in a comparable or greater extent than the Cr(VI) to Cr(III) reaction. In this case, the potential for Cl_2 evolution would be lowered to the range of the measured OCP. Considering that these reactions take place inside the polymer film and that chromate and Cl^- ions are present at very low concentrations (even traces), in addition to the fact that the distribution of reactants and products [e.g., Cr(III)] in the reaction media (i.e., the polymer film) is still unknown, it is very difficult to establish the exact mechanism and estimate proper potentials of the electrode reactions. Nonetheless, the possible production of Cl_2 and OCl^- species – accompanied by inhibited migration through the thick polymer film – are very likely events [48,49].

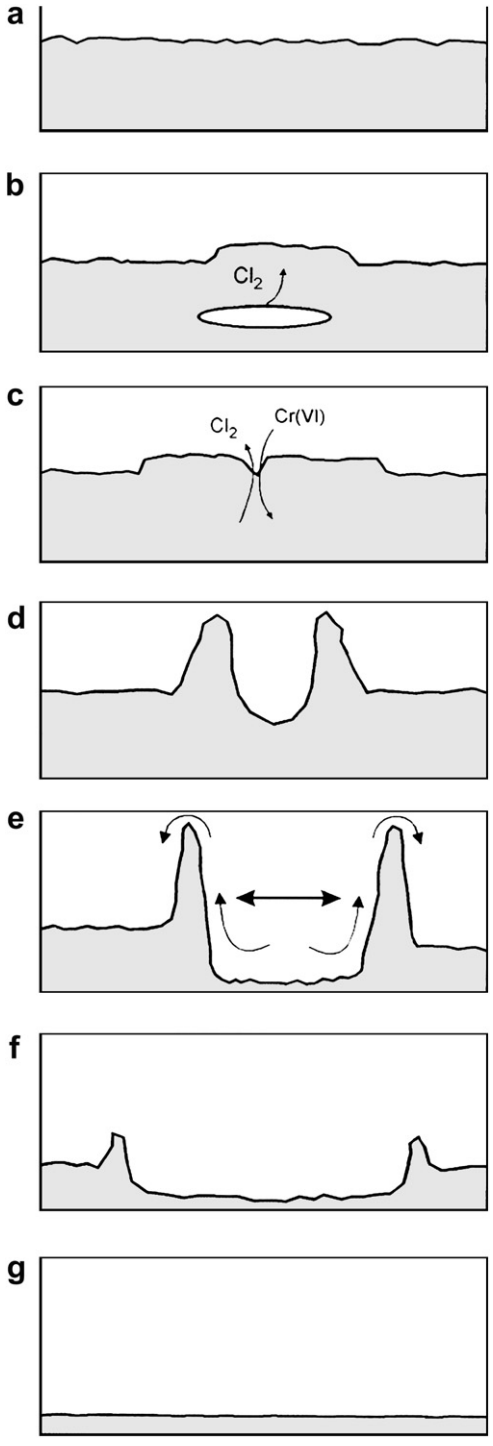

Fig. 8. Schematic pathway of the PPy film (a) multistep degradation, involving: polymer film bubbling (b); formation of donut-like structures (c and d); spreading of the circular features (e and f); and formation of an ultrathin film on the CV substrate (g).

In order to confirm the possibility of Cl_2 evolution in the PPy films and to estimate its influence on the polymer surface morphology, we performed a cyclic voltammetric scan of a freshly-prepared PPy film in an uncontaminated 0.1 M HCl solution. The scan started at −0.9 V vs. Ag/AgCl, and proceeded towards positive potentials. At potentials of 0.85–0.90 V vs. Ag/AgCl an increase in the electrode current was noticeable despite the absence of chromate in the electrolyte; this may be interpreted as a voltammetric peak connected with Cl_2 evolution. The sample was immediately taken out of the solution, rinsed with pure water and analyzed by AFM. Importantly, we found that the polymer surface was covered by circular structures identical to those previously found in the chromate-treated samples, which validates our model based on a significant role of the Cl^- ions in the formation of the circular polymer structures as part of the polymer film degradation process.

In order to further verify the hypothesized chlorine gas evolution due to the degradation of PPy films (containing residual Cl^-) during contact with Cr(VI) solutions, a PPy film grown on a vitreous carbon substrate was placed in contact with a chromate solution inside a capped conical vial. This vial was equipped with a U-shaped glass capillary connected to a NaOH solution trap (pH = 11.8). In this way, if chlorine gas were produced it would disproportionate into chloride and hypochlorite ions upon contact with the basic solution. The elution time of the ions contained in the resulting NaOH solution was compared in the ion chromatograph to that of a chloride ion standard. As shown in Fig. 9, both elution times are essentially identical.

The stability of the gas-caused polymer bubbles seems to be low, since they easily burst due to out-gassing. The Cr(VI)/Cr(III) inward/outward transport throughout the polymer film may also play a role here (see for example the influence of inward/outward transport of TiO_2 particles throughout a PPy film [50]). In this process, donut-shaped features are observed by AFM and optical microscopy (Fig. 8c). In a second step, a growth of circular polymer features via enlargement of the inner circular space (Fig. 8d–f) is observed. All the circular features appear to grow owing to material transport from the bottom of the inner space to the outside walls. Plausible

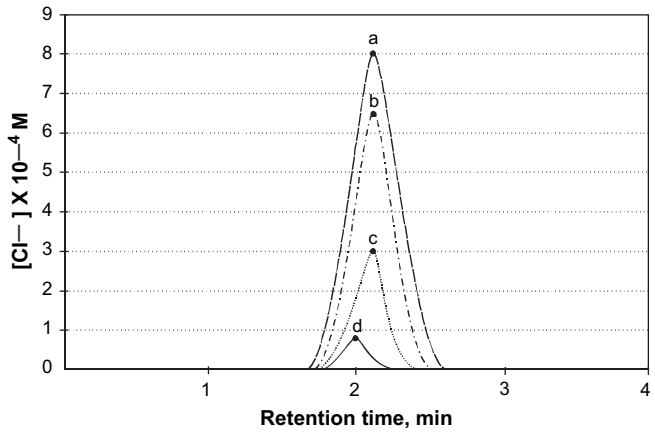

Fig. 9. Elution peaks of a chloride ion standard and of the product of the reaction between Cl^--containing PPy and a Cr(VI) solution. (a) Chloride ion standard, 8.1×10^{-4} M. (b) Chromate ions + PPy (grown at 0.9 V vs. Ag/AgCl, 5 min). The resulting gas was bubbled in NaOH, pH = 11.8. (c) Chromate ions + PPy (grown by potential cycling at 200 mV/s, 40 cycles from −0.3 to +0.9 V vs. Ag/AgCl). The resulting gas was bubbled in NaOH, pH = 11.8. (d) Millipore water + NaOH (pH = 11.8).

causes of this process are electrostatic (i.e., local charge accumulation) or hydrophobic (interactions between the inner walls of the polymer circle). A similar mechanism explains the columnar structure formation on surfactant-doped polypyrrole film surfaces [51]. The enlargement process is limited by the available material (i.e., the total thickness of the polymer film). This is why circular features stop to grow and – in a further development – they preferably spread up until the polymer surface becomes flat again (Fig. 8g). As pointed out earlier, the CV substrate was found to be covered in the final stage with an ultrathin polymer layer, which does not show catalytic activity for Cr(VI) reduction. These findings and the corresponding discussion lead to the conclusion that the PPy surface morphology transformations during chromate reduction predominantly involve a mechanical deformation and perturbations of the polymer film, accompanied by a significant degree of material transport. The presence of Cl^- inside the polymer (trapped during film preparation and/or film recharging) exposed to the Cr(VI) solution is likely a major cause of the polymer film degradation process.

Similar circular features on the PPy film surface have been observed before, albeit under significantly different experimental conditions, i.e., PPy grown on Au-Mylar [52] and PPy grown from a hexafluorophosphate electrolytic solution on Pt [53]. Indeed, this last study shows that PPy films with different surface morphology and different conducting properties can be prepared by changing the electrolyte composition (i.e., by varying the accompanying anion). Therefore, the possibility that the emergence of circular structures on the PPy surface be the result of micro-changes in the internal conformation of the polymer network cannot be ruled out. Detailed investigations in this direction are in progress in our laboratory. Even though it would be very interesting from a fundamental point of view to monitor changes in the surface film morphology in the presence of different anions in the electrolyte solution, in particular without Cl^- anions, real wastewater without Cl^- ions is actually difficult to find.

In addition to the observations of the substrate's influence on the PPy film at the early stages of growth and the agglomeration of PPy grains at latter stages, we were also interested in imaging the different redox states of the films. To this end, all the films described above were analyzed by means of AFM imaging after preparation at 0.9 V. Under a positive potential, the PPy film is oxidized and becomes conductive due to the nature of the polymeric skeleton and to the high content of the anionic species inside the polymer phase (i.e., high doping level). Since our polymer films were prepared in a KCl solution, the doping species was the Cl^- anion. In addition, the PPy films prepared at 0.9 V are most probably in the so called "overoxidized" form [54–57]. In general, this means that the PPy polymer is exposed to irreversible oxidation in the solid state, where polarons and bipolarons are effectively attacked by nucleophiles [58,59]. The overoxidation effect seems to be enhanced in the halide anion-containing media, particularly in the presence of Cl^- anions. Since overoxidation is followed by a partial loss of the polymer conductivity, the overoxidized polymer films usually become less electrochemically active [60,61]. Aware of such disadvantages, we still formed our PPy film at 0.9 V since the literature described earlier states that this potential is appropriate for the catalytic effects vs. Cr(VI) ions. Obviously, the physical and electrochemical properties, as well as the surface morphology characteristics of the PPy films, depend to a large extent on the synthetic conditions and the electrolyte used [53].

4. Conclusions

AFM images of PPy films grown on vitreous carbon (CV) substrates during the environmentally-relevant reduction of Cr(VI) ions to Cr(III) evidenced the major morphological characteristics of the bare carbon substrate and of the PPy film surface, as well as the course of the polymer film degradation via a dissolution mechanism during each additional cycle of exposure to the Cr(VI)/Cr(III) reaction and recharge at negative potentials in a KCl electrolyte. The analysis of PPy films prepared at different electrosynthesis times shows that surface morphology characteristics strongly depend on polymer film thickness. The thinner films (i.e., early stages of growth) appear to mimic the substrate morphology. A size increase in the nodular polymer units was observed at later stages of growth. Surprisingly, the oxidized and reduced states of the PPy films do not show significant differences in their surface morphology. Thicker films (>2 μm) break more easily and detach from the carbon substrate. The thinner polymer films undergo a degradation process accompanied by formation of well-defined circular features (rings). Detailed analysis of the morphological characteristics of such PPy rings at different stages of chromate reduction has allowed us to propose a mechanism for the polymer degradation process. This process, accompanied by significant mass transfer and morphological perturbations, seems to be predominantly initiated by the development of gas bubbles (of Cl_2) inside the polymer phase. At later stages of film dissolution, the observed enlargement of the PPy rings is presumably due to the influence of electrostatic or hydrophobic repulsion forces between the inner walls of the rings. The last stage of the degradation process involves the formation of an ultrathin, catalytically inactive PPy film (with no signs of circular structures) that remains on the carbon surface even after prolonged treatment in chromate solution (i.e., 9 or more cycles).

Acknowledgment

We thank Jorge Mostany (U. Simon Bolivar, Venezuela) for helpful comments. Experimental assistance by Ulises Paramo, Elizabeth Garcia and Samuel Macias is gratefully acknowledged. Financial assistance was received from CONACYT (Mexico) and from Universidad Iberoamericana.

References

[1] Katz SA, Salem H. The toxicology of chromium with respect to its chemical speciation: a review. J Appl Toxicol 1993;13(3):217–24.
[2] Alcedo JA, Wetterhann KE. Chromium toxicity and carcinogenesis. Int Rev Exp Pathol 1990;31:85–108.

[3] Schroeder DC, Lee GE. Potential transformations of chromium in natural waters. Water Air Soil Pollut 1975;4(3–4):355–65.
[4] Mayer LM, Schick LL. Removal of hexavalent chromium from estuarine waters by model substrates and natural sediments. Environ Sci Technol 1981;15(12):1482–4.
[5] Kieber RJ, Helz GR. Indirect photoreduction of aqueous chromium(VI). Environ Sci Technol 1992;26(2):307–12.
[6] Rai D, Sass BM, Moore DA. Chromium(III) hydrolysis constants and solubility of chromium(III) hydroxide. Inorg Chem 1987;26(3):345–9.
[7] Wittbrodt PR, Palmer CD. Reduction of Cr(VI) in the presence of excess soil fulvic acid. Environ Sci Technol 1995;29(1):255–63.
[8] Elovitz MS, Fish W. Redox interactions of Cr(VI) and substituted phenols: kinetic investigation. Environ Sci Technol 1994;28(12):2161–9.
[9] Agarwal IC, Rochon AM, Gesser HD, Sparling AB. Electrodeposition of six heavy metals on reticulated vitreous carbon electrode. Water Res 1984;18(2):227–32.
[10] Kuhn AT. Electrochemical techniques for effluent treatment. Chem Ind 1971;34:946–50.
[11] Rajeshwar K, Ibanez JG, Swain GM. Electrochemistry and the environment. J Appl Electrochem 1994;24(11):1077–91.
[12] Senthurchelvan R, Wang Y, Basak S, Rajeshwar K. Reduction of hexavalent chromium in aqueous solutions by polypyrrole. II. Thermodynamic, kinetic, and mechanistic aspects. J Electrochem Soc 1996;143(1):44–51.
[13] Wei C, German S, Basak S, Rajeshwar K. Reduction of hexavalent chromium in aqueous solutions by polypyrrole. J Electrochem Soc 1993;140(4):L60–2.
[14] Rodríguez FJ, Gutiérrez S, Ibanez JG, Bravo JL, Batina N. The efficiency of toxic chromate reduction by a conducting polymer (polypyrrole): influence of electropolymerization conditions. Environ Sci Technol 2000;34:2018–23.
[15] Guzman-Pantoja J, Ibanez JG, Vasquez-Medrano RC, Oropeza-Guzman MT. Direct electrochemical reduction of hexavalent chromium in a filter-press reactor. Bull Electrochem 2004;20(3):107–14.
[16] Rodríguez-Valadez F, Ortiz-Éxiga C, Ibanez JG, Alatorre-Ordaz A, Gutiérrez-Granados S. Electroreduction of Cr(VI) to Cr(III) on reticulated vitreous carbon electrodes in a parallel-plate reactor with recirculation. Environ Sci Technol 2005;39:1875–9.
[17] (a) Alatorre MA, Páramo U, Gutiérrez-Granados S, Ibanez JG. Surface modification of polypyrrole deposited on vitreous carbon due to charge–discharge–contact cycles with Cr(VI). XI meeting of the Mexican Electrochemical Society; Oct 1996. (b) Alatorre MA, Páramo U, Gutiérrez-Granados S, Ibanez JG. Reduction of hexavalent chromium by polypyrrole deposited on large surface porous electrodes. XII Iberoamerican Electrochemistry Congress, Mérida, Venezuela, Mar 24–29; 1996.
[18] Fernandez LF, Ibanez JG, Rajeshwar K, Basak S. The reduction of Cr(VI) with polypyrrole on reticulated vitreous carbon: miscellaneous effects. Abstract no. 524, 189th meeting of The Electrochemical Society, Los Angeles, California, May 5–10; 1996.
[19] Alatorre A, Gutiérrez-Granados S, Páramo U, Ibanez JG. Reduction of hexavalent chromium by polypyrrole deposited on different carbon substrates. J Appl Electrochem 1998;28:551–7.
[20] Maksymiuk K. Chemical reactivity of polypyrrole and its relevance to polypyrrole based electrochemical sensors. Electroanalysis 2006;18(16):1537–51.
[21] Otero TF, Marquez M, Suarez IJ. Polypyrrole: diffusion coefficients and degradation by overoxidation. J Phys Chem B 2004;108(39):15429–33.
[22] Rodriguez I, Scharifker BR, Mostany J. In situ FTIR study of redox and overoxidation processes in polypyrrole films. J Electroanal Chem 2000;491(1–2):117–25.
[23] Park DS, Shim YB, Park SM. Degradation kinetics of polypyrrole films. J Electrochem Soc 1993;140(10):2749–52.
[24] Park DS, Shim YB, Park SM. Degradation of electrochemically prepared polypyrrole in aqueous sulfuric acid. J Electrochem Soc 1993;140(3):609–14.
[25] Schlenoff JB, Xu H. Evolution of physical and electrochemical properties of polypyrrole during extended oxidation. J Electrochem Soc 1992;139(9):2397–401.
[26] Chehimi MM, Abdeljalil E. A study of the degradation and stability of polypyrrole by inverse gas chromatography, X-ray photoelectron spectroscopy, and conductivity measurements. Synth Met 2004;145(1):15–22.
[27] Kaynak A. Aging studies on conducting polypyrrole. Fibers Polym 2001;2(4):171–7.
[28] Geffroy B, Breivik L, Corbel C, Kauppinen H, Liszkay L, Barthe M-F. Aging effects in polypyrrole probed by positron annihilation. Synth Met 1999;101(1–3):383–4.
[29] Jolly R, Pairis S, Petrescu C. Aging compared in three polymer conductors. J Chim Phys Phys-Chim Biol 1998;95(6):1400–5.
[30] Mathys GI, Truong V-T. Spectroscopic study of thermo-oxidative degradation of polypyrrole powder by FT-IR. Synth Met 1997;89(2):103–9.
[31] Burford RP, Moss BK, Lamb R. Degradation of electrodeposited polypyrroles. J Intell Mater Syst Struct 1994;5(6):749–57.
[32] Thieblemont JC, Planche MF, Petrescu C, Bouvier JM, Bidan G. Kinetics of degradation of the electrical conductivity of polypyrrole under thermal aging. Polym Degrad Stab 1994;43(2):293–8.
[33] Tansley TL, Maddison DS. Conductivity degradation in oxygen-aged polypyrrole. J Appl Phys 1991;69(11):7711–3.
[34] Moss BK, Burford RP. A kinetic study of polypyrrole degradation. Polymer 1992;33(9):1902–8.
[35] Vork FTA, Ubbink MT, Janssen LJJ, Barendrecht E. Degradation of polypyrrole-modified electrodes in a chloride containing medium. Recl Trav Chim Pays-Bas 1985;104(7–8):215–6.
[36] Neoh KG, Lau KKS, Wong VVT, Kang ET, Tan KL. Structure and degradation behavior of polypyrrole doped with sulfonate anions of different sizes subjected to undoping–redoping cycles. Chem Mater 1996;8(1):167–72.
[37] Cataldo F, Omastova M. On the ozone degradation of polypyrrole. Polym Degrad Stab 2003;82(3):487–95.
[38] Gao J, Tian Z, Xue Q. In situ time-resolved Raman spectroscopic studies of redox process and degeneration of PPy electrodes in solutions with various pH. Guangpuxue Yu Guangpu Fenxi 1996;16(1):47–53.
[39] Kappen P, Hale PS, Brack N, Prissanaroon W, Pigram PJ. X-PEEM/NEXAFS and AFM of polypyrrole and copper micro-patterns on insulating fluoropolymer substrates. Appl Surf Sci 2006;253(3):1473–9.
[40] Mazeikiene R, Malinauskas A. Kinetics of the electrochemical degradation of polypyrrole. Polym Degrad Stab 2002;75(2):255–8.
[41] Rodriguez FJ, Garcia de la Rosa LA, Alatorre A, Ibanez JG, Godinez L, Gutierrez S, et al. Analysis of the effect of polypyrrole synthesis conditions on its capacity to reduce hexavalent chromium. Prog Org Coat 2007;60:297–302.
[42] Guzman J, Ibanez JG. Electrically aided production of a conducting polymer on porous electrodes. Afinidad (Spain) 2005;62(519):469–72.
[43] McDermott MT, McDermott CA, McCreery R. Scanning tunneling microscopy of carbon surfaces: relationships between electrode kinetics, capacitance, and morphology for glassy carbon electrodes. Anal Chem 1993;65(7):937–44.
[44] Wang J, Martinez T, Yanin DR, McCormick LD. Scanning tunneling microscopic investigation of surface fouling of glassy carbon surfaces due to phenol oxidation. J Electroanal Chem Interf Electrochem 1991;313(1–2):129–40.
[45] Gandhi M, Spinks GM, Burford RP, Wallace GG. Film substructure and mechanical properties of electrochemically prepared polypyrrole. Polymer 1995;36(25):4761–5.
[46] Li J, Wang E, Green M, West PE. In situ AFM study of the surface morphology of polypyrrole film. Synth Met 1995;74(2):127–31.
[47] Bard AJ, Faulkner LR. Electrochemical methods: fundamentals and applications. New York: Wiley; 1980.
[48] Chen CC, Rajeshwar K. Chemical attack on polypyrrole by electrolytically generated solution species in aqueous chloride medium. J Electrochem Soc 1994;141(11):2942–6.
[49] Ibanez JG, Alatorre A, Páramo U, Batina N. Study of the degradation of polypyrrole films during the reduction of chromate ions by atomic force

microscopy. In: Walton CW, Rudd EJ, editors. Proceedings of energy and electrochemistry processes for a cleaner environment, vol. PV97-28. New Jersey: The Electrochemical Society; 1998. p. 61–71.
[50] Beck F, Dahlhaus M, Zahedi N. Anodic codeposition of polypyrrole and dispersed titanium dioxide. Electrochim Acta 1992;37(7):1265–72.
[51] Naoi K, Oura Y, Maeda M, Nakamura S. Electrochemistry of surfactant-doped polypyrrole film (I): Formation of columnar structure by electropolymerization. J Electrochem Soc 1995;142(2):417–22.
[52] Spinks G. Technical brochure. AFM image, University of Wollongong, Australia. USA: Park Scientific Instruments; March, 1996.
[53] Salmon M, Diaz AF, Logan AJ, Krounbi M, Bargon J. Chemical modification of conducting polypyrrole films. Mol Cryst Liq Cryst 1982;83(1–4):1297–308.
[54] Novak P. Limitations of polypyrrole synthesis in water and their causes. Electrochim Acta 1992;37(7):1227–30.
[55] Christensen PA, Hamnett A. In situ spectroscopic investigations of the growth, electrochemical cycling and overoxidation of polypyrrole in aqueous solution. Electrochim Acta 1991;36(8):1263–86.
[56] Fermin DJ, Teruel H, Scharifker BR. Changes in the population of neutral species and charge carriers during electrochemical oxidation of polypyrrole. J Electroanal Chem 1996;401(1–2):207–14.
[57] Mostany J, Scharifker BR. Direct microcalorimetric measurement of doping and overoxidation processes in polypyrrole. Electrochim Acta 1996;42(2):291–301.
[58] Beck F, Braun P, Oberst M. Organic electrochemistry in the solid state – overoxidation of polypyrrole. Berichte der Bunsen-Gesellschaft 1987;91(9):967–74.
[59] Ko JM, Rhee HW, Park S-M, Kim CY. Morphology and electrochemical properties of polypyrrole films prepared in aqueous and nonaqueous solvents. J Electrochem Soc 1990;137(3):905–9.
[60] Mengoli G, Musiani MM, Fleischmann M, Plecher D. Studies of pyrrole black electrodes as possible battery cathodes. J Appl Electrochem 1984;14(3):285–91.
[61] Novak P, Rasch B, Viestlich W. Overoxidation of polypyrrole in propylene carbonate. An in situ FTIR study. J Electrochem Soc 1991;138(11):3300–4.